Supporting information for

In-Situ Fabricated NiCo-MOF@NiCo Acetate Hydroxide Composites with Hollow Structure for Enhanced Electrochemical Performance in Aqueous Nickel-Zinc Batteries

Ziming Qiu,[a] Xingye Lu,[a] Yexi Fan,[a] Xinling Lv,[ac] Wanchang Feng,[ad] Zefan Sang,[a] Shixian Wang,[a] Bingyi Yan,[ae] Mohsen Shakouri,[b] and Huan Pang[a]*

a. School of Chemistry and Chemical Engineering, Yangzhou University, Yangzhou, 225002 Jiangsu, P. R. China. E-mail: huanpangchem@hotmail.com (H. Pang)
b. Canadian Light Source Inc., University of Saskatchewan Saskatoon, S7N 2V3, Canada
c. Interdisciplinary Research Center for Advanced Energy, Yangzhou University, Yangzhou, Jiangsu 225127, P. R. China
d. School of Chemistry and Chemical Engineering, Chongqing University of Science and Technology, Chongqing, 401331, P. R. China
e. School of Environmental Science, Nanjing Xiaozhuang University, Nanjing, Jiangsu, 211171, P. R. China

Experimental Section:

Chemicals. Cobalt(II) acetate tetrahydrate ($Co(CH_3COO)_2 \cdot 4H_2O$), Nickel(II) acetate tetrahydrate ($Ni(CH_3COO)_2 \cdot 4H_2O$), 2,5-dimethylterephthalic acid ($C_{10}H_{10}O_4$), and polyvinylpyrrolidone ($(C_6H_9NO)n$, M.W.～58,000) were purchased from Shanghai Aladdin Biochemical Technology Co., Ltd., China. N,N-Dimethylformamide (DMF) and ethanol (CH_3CH_2OH) was purchased from Sinopharm Chemical Reagent Co., Ltd., China. All the chemicals were used as received without further purification. DI water (18 MΩ/cm) used in all experiments was prepared by passing through an ultra-pure purification system.

Synthesis of NiCo AHP. Typically, 1.0 g polyvinylpyrrolidone (PVP), 160 mg $Co(CH_3COO)_2 \cdot 4H_2O$, and 480 mg $Ni(CH_3COO)_2 \cdot 4H_2O$ were first dissolved in 200 mL of ethanol at room temperature to form a clear pink solution, and then heated under stirring conditions and kept at 85 °C for 2 h, washed three times with ethanol, and dried under vacuum for 12 h. The synthesis of other Ni/Co ratios is similar to that of the NiCo AHP, differing only in the proportions of metal salts used during synthesis. In the syntheses of H-Ni-MOF@AHC, H-$Ni_{0.67}Co_{0.33}$-MOF@AHC, and H-$Ni_{0.5}Co_{0.5}$-MOF@AHC, 640 mg $Ni(CH_3COO)_2 \cdot 4H_2O$, 213.3 mg $Co(CH_3COO)_2 \cdot 4H_2O$/426.7 mg $Ni(CH_3COO)_2 \cdot 4H_2O$, and 320 mg $Co(CH_3COO)_2 \cdot 4H_2O$/320 mg $Ni(CH_3COO)_2 \cdot 4H_2O$ were respectively introduced.

Synthesis of H-NiCo-MOF@AHC. In a typical synthesis, 100 mg NiCo AHP and 118mg 2,5-dimethylterephthalic acid were dispersed in 10 mL and 150 mL of DMF, respectively. Then, the NiCo-containing solution was quickly added to the other one and stirred at 95 °C for 2 h. Subsequently, the resulting NiCo-MOF@AHC samples were rapidly centrifuged and collected, then washed several times with ethanol. The synthesis procedures for NiCo-MOF@AHP and NiCo-MOF were similar to that of NiCo-MOF@AHC, with the exception of the reaction time. For the synthesis of NiCo-MOF@AHP, the reaction time was 1 hour; for the synthesis of NiCo-MOF, the reaction time was 4 hours.

Characterizations. The Powder X-ray diffraction (PXRD) patterns were performed by Bruker AXS D8 advance with Cu Kα radiation of 40 kV (λ=1.5418 Å). Transmission electron microscopy (TEM) and Energy Dispersive Spectrometer (EDS) elemental mapping scans were recorded using Tecnai G2 F30 S-TWIN at an acceleration voltage of 300 kV. XPS analysis was carried out using a Thermo Scientific ESCALAB 250Xi X-ray photoelectron spectrometer with Al Kα radiation of 1486.6 eV as the excitation source, the survey thickness is 2 - 3 nm. The reference for calibration is the peak of C 1s at 284.8 eV.

Preparation of working electrodes. The active material, acetylene black and polyvinylidene difluoride (PVDF) were thoroughly mixed in N-methylpyrrolidone (NMP) at a weight ratio of 8:1:1. The formed slurry was then sonicated for 30 min before being deposited on a 1 cm × 2 cm carbon cloth, ensuring that the sample was coated within a 1 cm × 1 cm area. The carbon cloth was subsequently placed in a vacuum oven at 60 °C for at least 12 h before electrochemical testing. The loading of active material was approximately 2.5 mg cm^{-2}.

Electrochemical performance testing. Three-electrode system: H-NiCo-MOF, H-NiCo-MOF@AHC, and H-NiCo-MOF@AHP electrodes respectively (1 cm × 2 cm, loading per unit area of 2.5 mg cm^{-2}) were tested for electrochemical performance using an electrochemical workstation (CHI 660E) in an aqueous electrolyte of KOH (3 M). Pt wire was used as the counter electrode, and the Hg/HgO electrode was used as the reference electrode.

Two-electrode systems: H-NiCo-MOF//Zn, H-NiCo-MOF@AHC//Zn, and H-NiCo-MOF@AHP//Zn cells were simulated in an electrolyzer using 3 M KOH containing 20 mM zinc acetate ($Zn(Ac)_2$) as the electrolyte, H-NiCo-MOF, H-NiCo-MOF@AHC, and H-NiCo-MOF@AHP (1 cm × 2 cm) as the positive electrode, and Zn sheet (1 cm × 3 cm) was the negative electrode. Prior to electrochemical testing, the prepared cells were subjected to an electrochemical activation process with 20 cyclic voltammetry tests.

Cyclic voltammetric curve (CV) test: Cyclic voltammetry is one of the most important methods to study the electrochemical properties of electrode materials, such as the occurrence of redox reactions and the reversibility of electrochemical reactions, and it is widely used in the study of batteries. Cyclic voltammetry test was performed to activate the working electrode before the start of other tests, with a scan rate of 5 mV s-1, a scan range of 0 - 0.6 V in the three electrode system. Observe the trend of the curve, when the phenomenon of gradual overlap is presented, the electrode has been activated to a stable state, and the next test can be carried out.

Constant current charge/discharge (GCD) test: Constant-current charging and discharging is an important method to study the performance of electrode materials in terms of charging and discharging time, discharge specific capacity, Coulombic efficiency, multiplicity performance, cycle life and cycle stability, etc. The charging and discharging voltage range of nickel-zinc batteries is generally 1.4 - 2.1 V. However, the charging cut-off voltage will be finely adjusted according to the amount of current density that can be achieved by the materials. The cycle stability test was conducted within a voltage range of 1.4 V to 1.95V, using a constant charge/discharge current of 5 mA cm^{-2}.

The specific capacity Ca (mAh cm^{-2}) of the working electrode in the three-electrode system is calculated from the discharge curve according to the following equation:

$$C_a = \frac{I \times \Delta t}{S}$$

where I (mA) is the discharge current, Δt (h) is the discharge time, and S (cm^2) is the electrode area.

The average energy density (E) and average power density (P) of the battery were calculated by the following equations:

$$E = \frac{I\int_0^{\Delta t} U(t)dt}{S}$$

$$P = \frac{E}{\Delta t}$$

where E (mW h cm^{-2}) is the surface energy density, I (mA) is the discharge current, U (t) is the voltage (V) during discharge, dt is the time difference, Δt (h) is the discharge time, S (cm^2) is the total surface area of the MOFs//Zn battery, and P (mW cm^{-2}) is the surface power density.

The kinetic of capacitive contribution can be obtained through calculating the CV curves at different scan rates. The relationship between current (i) and scan rate (v) can be written as:

$$i = av^b$$

$$\log(i) = \log(a) + blog(v)$$

where a and b are constant can be obtained from log(v) versus log(i) plots. When b = 0.5 represents an ideal diffusion-controlled process, and b = 1.0 indicates a surface capacitive-controlled process.

The ratio of capacitive contributions can be further described by the following equation: $i = k_1v + k_2v^{1/2}$, where k_1v and $k_2v^{1/2}$ correspond to capacitive and diffusive contributions, respectively.

Electrochemical Impedance Spectroscopy (EIS) test: The electrochemical impedance (EIS) test is performed at an open-circuit voltage with an AC frequency range of 105 to 0.01 Hz and an amplitude of 5 mV. The smaller the impedance obtained by the test, the more efficient the electron transfer and the faster the reaction rate. The impedance curve generally consists of a semicircle (high-frequency region, charge-transfer dominated) and a diagonal line (low-frequency region, matter-transfer controlled), with the size of the semicircle radius representing the magnitude of the impedance of the carriers in the migration process.

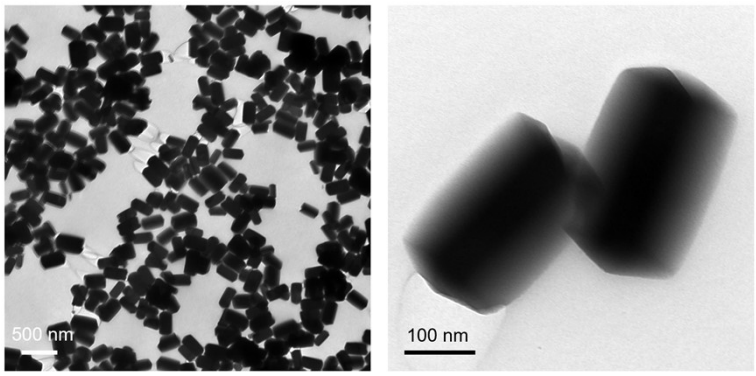

Fig. S1 TEM images of $Ni_{0.75}Co_{0.25}$ AHP.

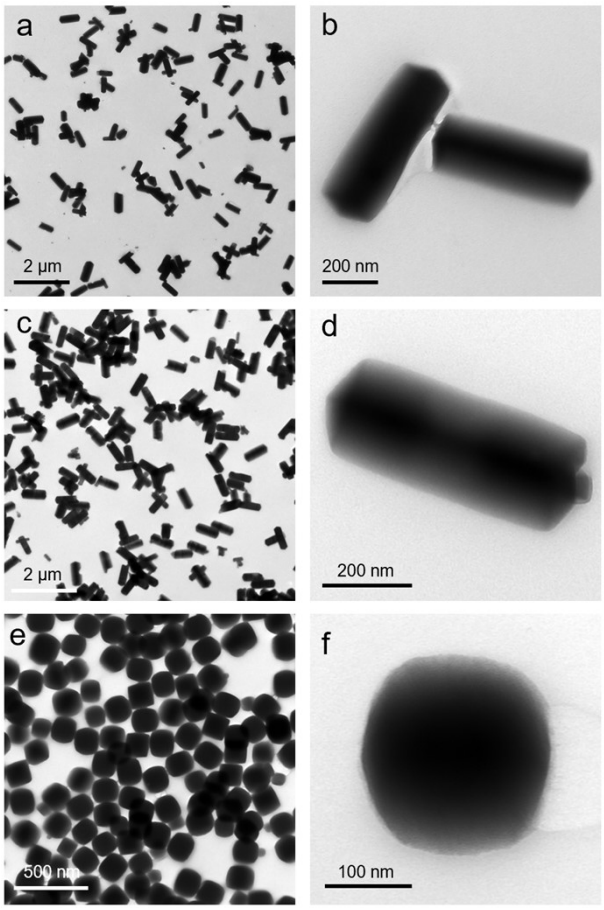

Fig. S2 TEM images of (a, b) $Ni_{0.5}Co_{0.5}$ AHP, (c, d) $Ni_{0.67}Co_{0.33}$ AHP, and (e, f) Ni AHP.

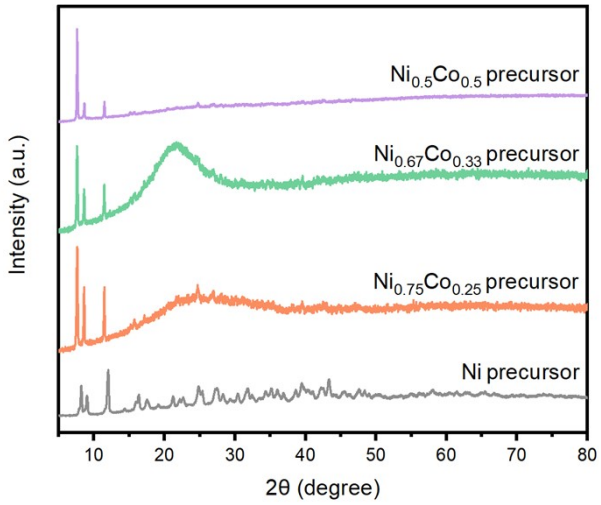

Fig. S3 XRD pattern of $Ni_{0.5}Co_{0.5}$ AHP, $Ni_{0.67}Co_{0.33}$ AHP, $Ni_{0.75}Co_{0.25}$ AHP, and Ni AHP.

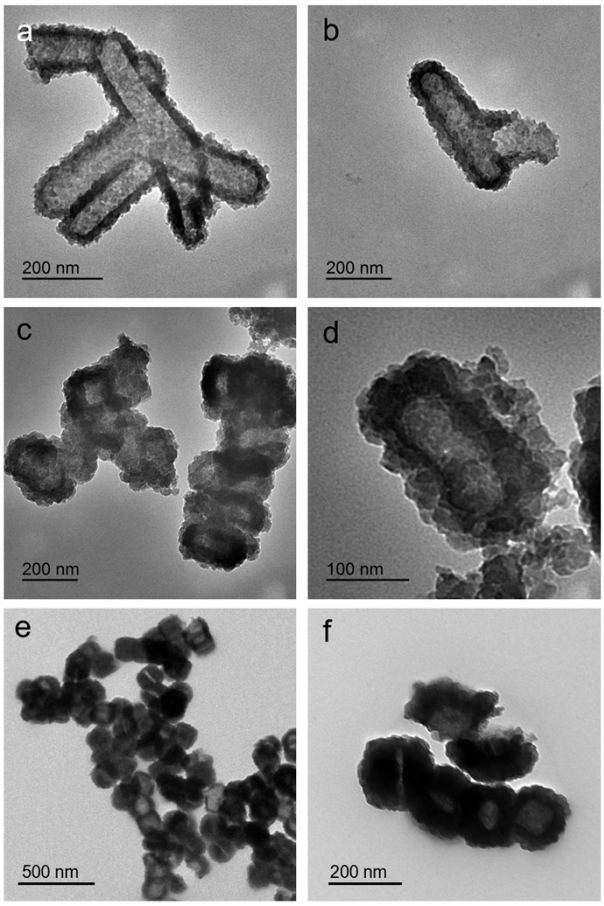

Fig. S4 TEM images of (a, b) H-$Ni_{0.5}Co_{0.5}$-MOF, (c, d) H-$Ni_{0.67}Co_{0.33}$-MOF@AHC, and (e, f) H-Ni-MOF@AHC.

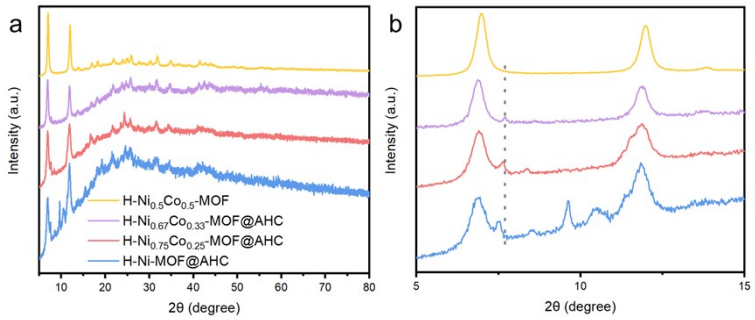

Fig. S5 XRD pattern of H-$Ni_{0.5}Co_{0.5}$-MOF, H-$Ni_{0.67}Co_{0.33}$-MOF@AHC, H-NiCo-MOF@AHC, and H-Ni-MOF@AHC.

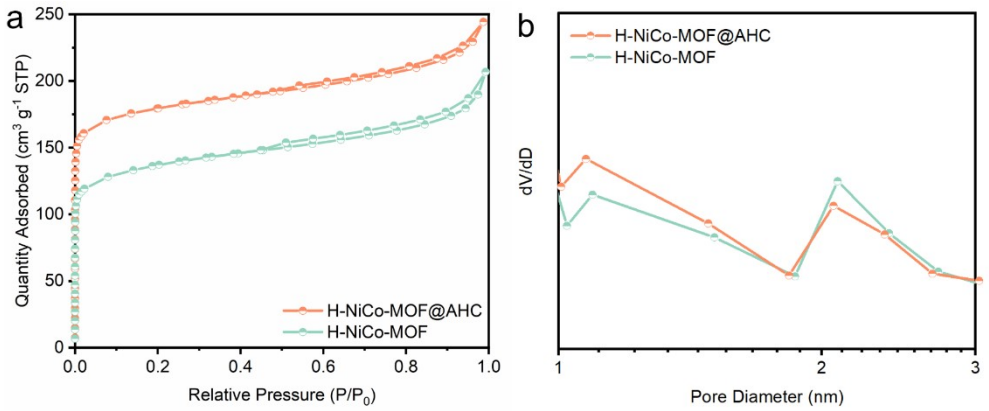

Fig. S6 (a) N_2 adsorption-desorption isotherms and (b) pore size distributions of H-NiCo-MOF@AHC and H-NiCo-MOF.

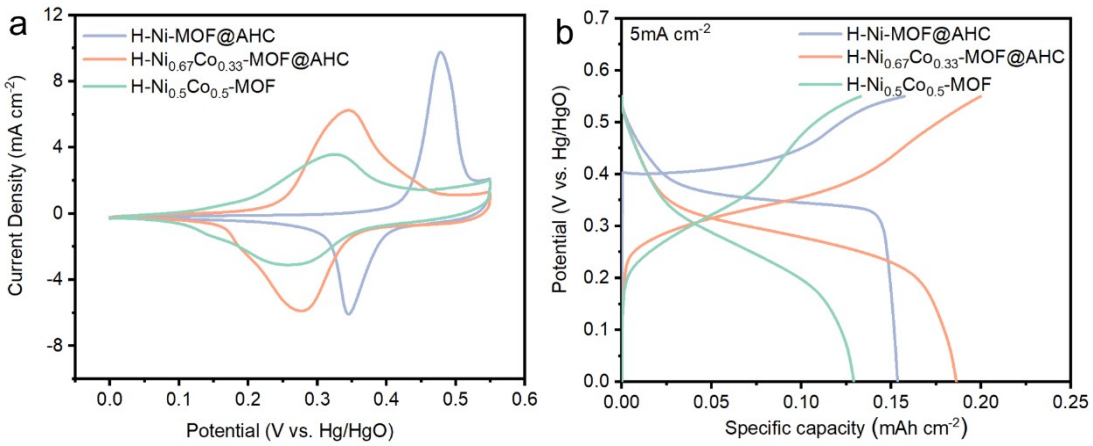

Fig. S7 (a) CV curves at 1 mV s^{-1} and (b) GCD at 5 mA cm^{-2} of H-Ni-MOF@AHC, H-$Ni_{0.67}Co_{0.33}$-MOF@AHC, and H-$Ni_{0.5}Co_{0.5}$-MOF.

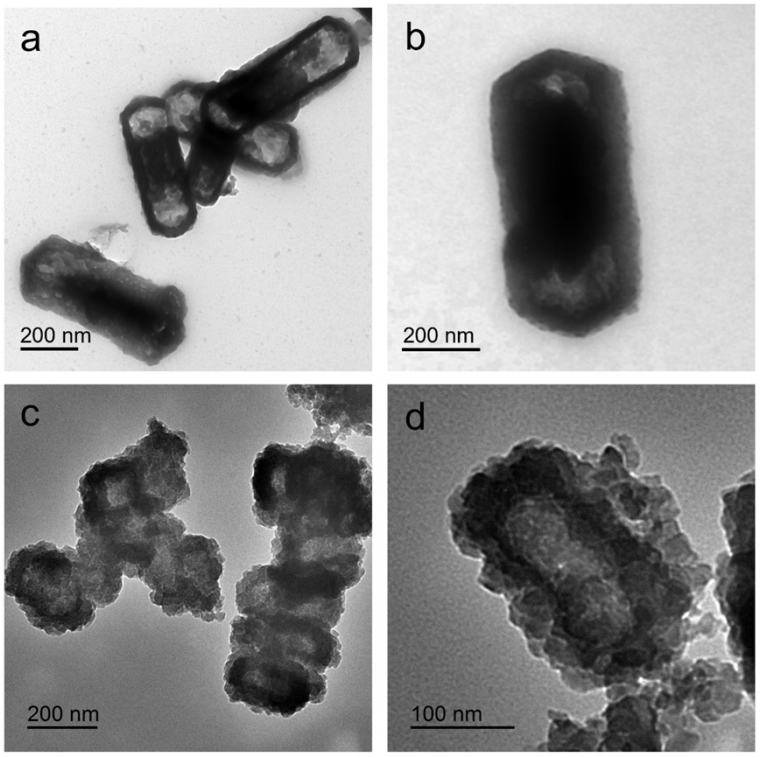

Fig. S8 TEM images of (a, b) H-NiCo-MOF@AHP and (c, d) H-NiCo-MOF.

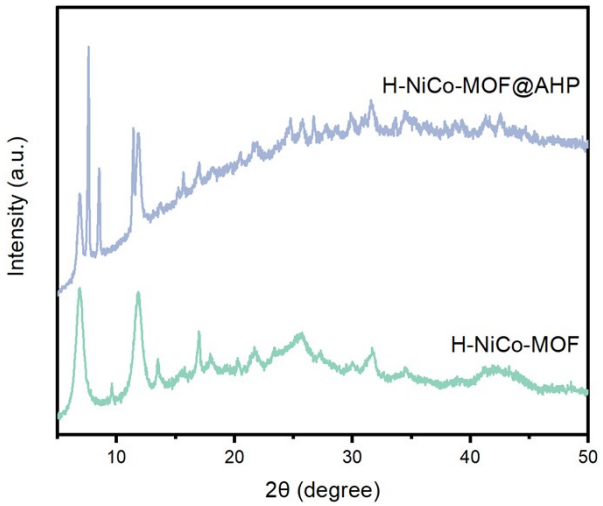

Fig. S9 XRD pattern of H-NiCo-MOF@AHP and H-NiCo-MOF.

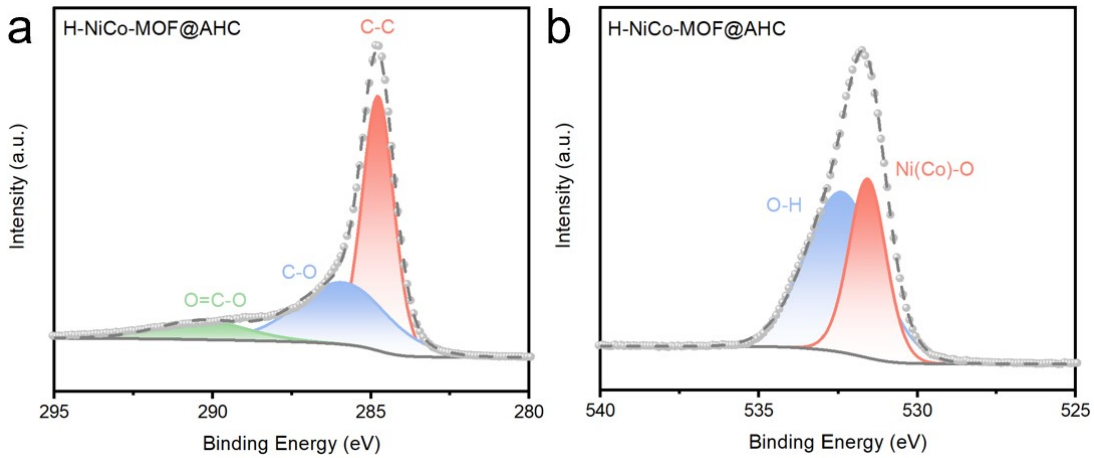

Fig. S10 (a) C 1s and (b) O 1s XPS spectra of H-NiCo-MOF@AHC.

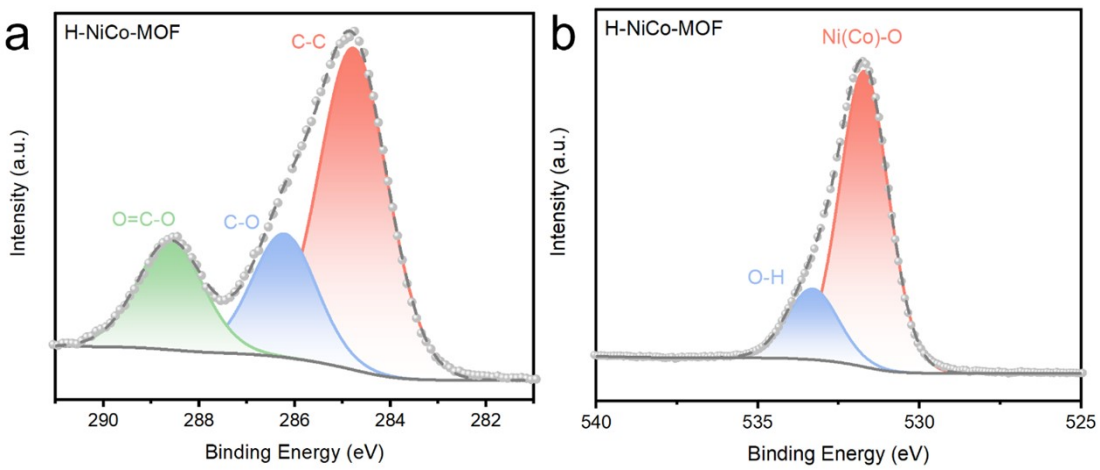

Fig. S11 (a) C 1s and (b) O 1s XPS spectra of H-NiCo-MOF.

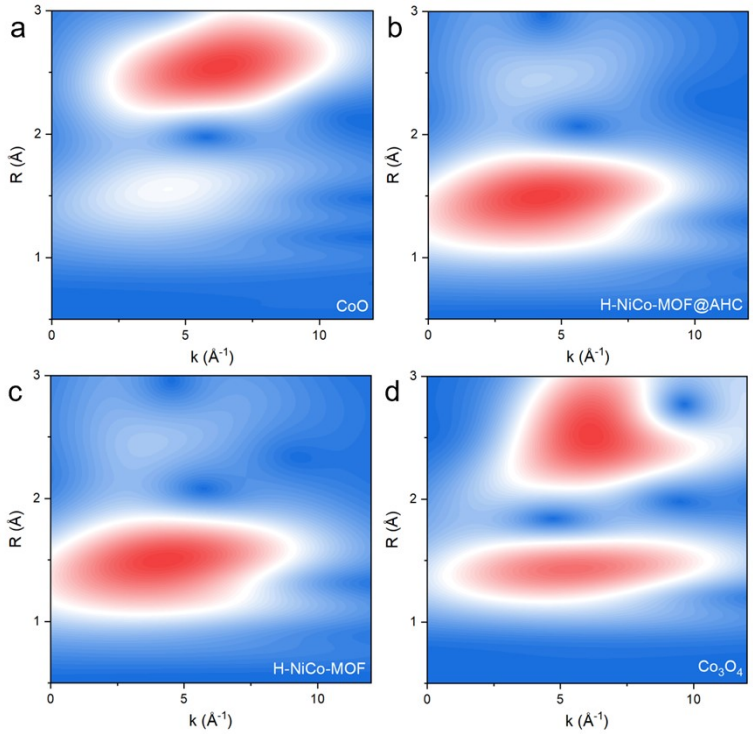

Fig. S12 Co K-edge WT-EXAFS of (a) CoO, (b) H-NiCo-MOF@AHC, (c) H-NiCo-MOF, and Co_3O_4.

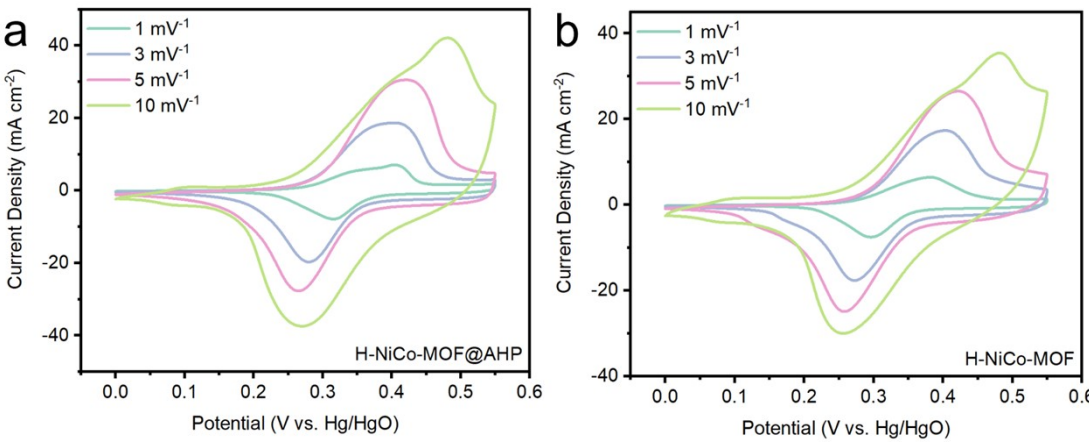

Fig. S13 CV curves of (a) H-NiCo-MOF@AHP and (b) H-NiCo-MOF at 1-10 mV s^{-1}.

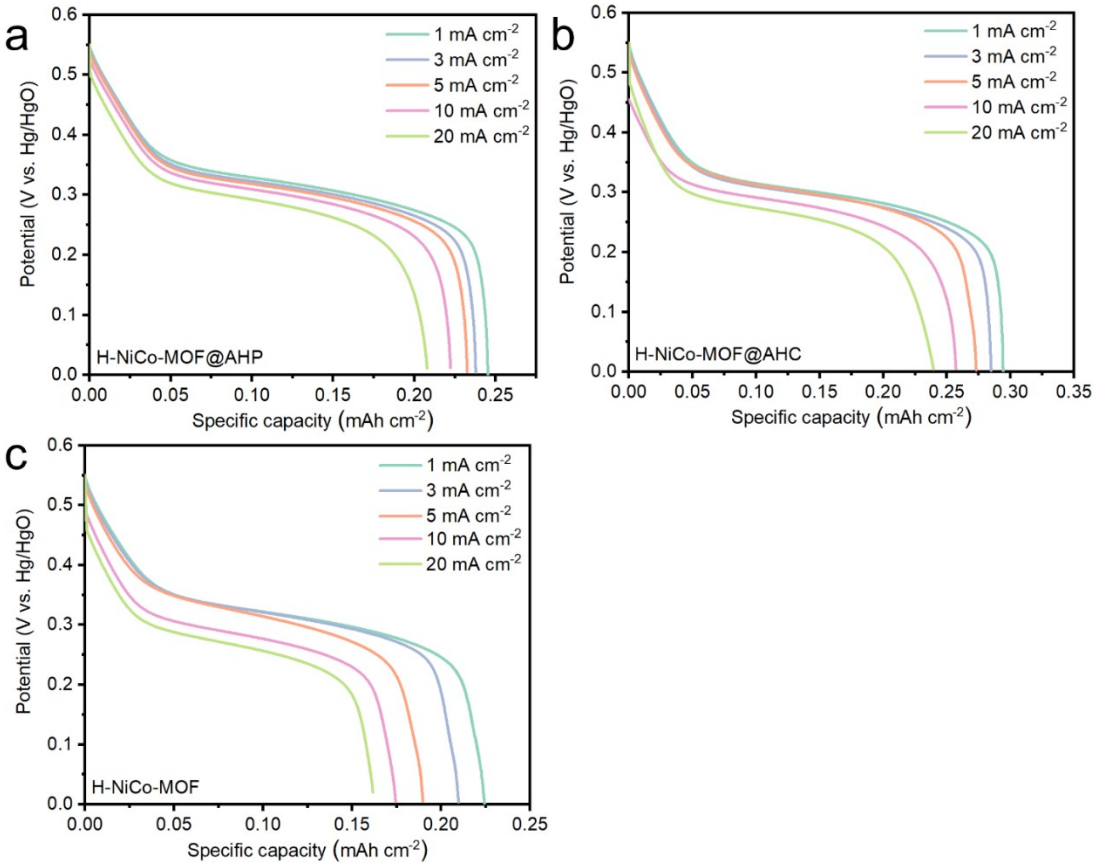

Fig. S14 Discharge curves (a) H-NiCo-MOF@AHP, (b) H-NiCo-MOF-AHC, and (c) H-NiCo-MOF at 5 mA cm^{-2}.

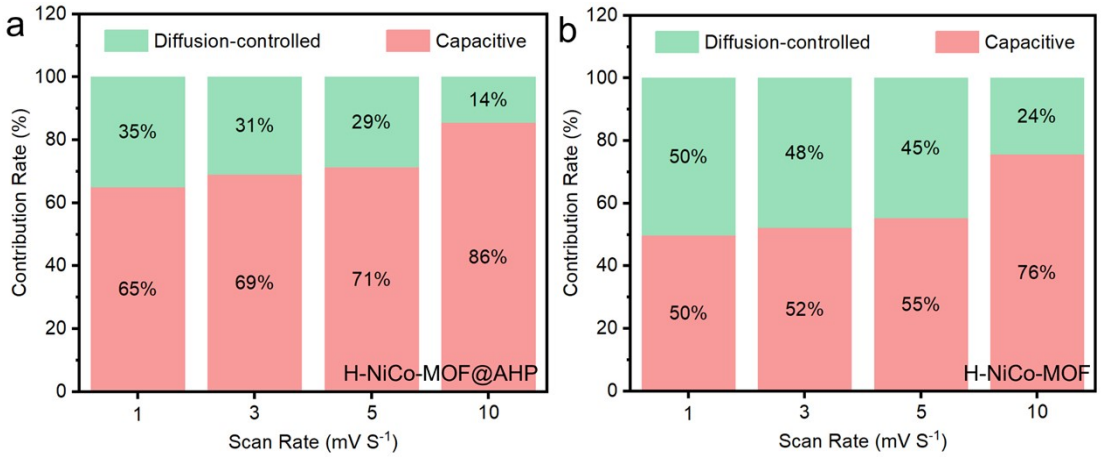

Fig. S15 The ratio of capacitive and diffusion-controlled contribution (a) H-NiCo-MOF@AHP and (b) H-NiCo-MOF at various scan rates.

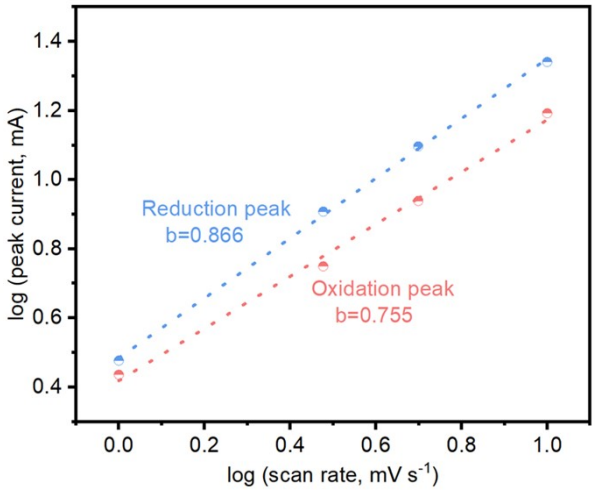

Fig. S16 Linear fitting of the peak current of the REDOX peak and the scanning rate in the CV curve of H-NiCo-MOF@AHC//Zn electrodes.

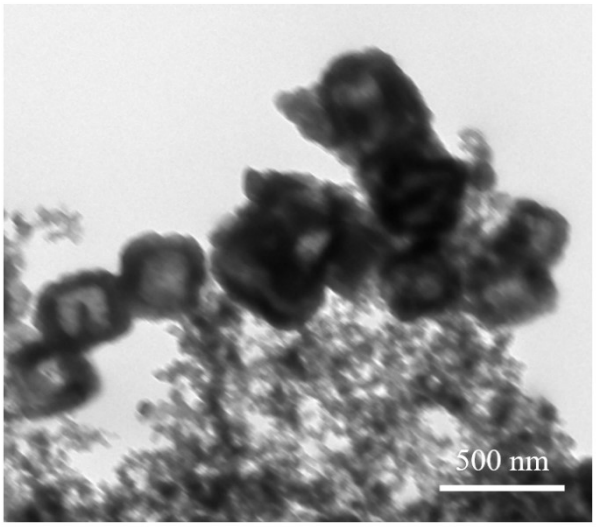

Fig. S17 TEM image of H-NiCo-MOF@AHC after long-term cycling.

Table S1. The equivalent circuit and fitted electrochemical kinetic parameters of H-NiCo-MOF@AHP//Zn, H-NiCo-MOF@AHC//Zn, and H-NiCo-MOF//Zn samples.

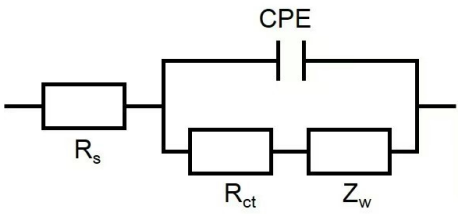

Samples	Rs (Ω)	Rct (Ω)
H-NiCo-MOF@AHP//Zn	1.522	0.32
H-NiCo-MOF@AHC//Zn	1.388	0.081
H-NiCo-MOF//Zn	1.737	0.084

Table S2. Comparison of energy/power densities between H-NiCo-MOF@AHC//Zn battery with other previously reported works.

Electrode materials	E_A [a] (mWh cm^{-2})	E_G [b] (Wh kg^{-1})	Reference
β-$Ni(OH)_2$ nanocube	~0.016 at 5.612 mW cm^{-2}	/	[1]
$NiCo_2O_4$	/	85.8 at ~1 kW kg^{-1}	[2]
MH-Ni_4Co_1//Zn@CC	0.613 at 32.89 mW cm^{-2}	/	[3]
GF/CNTs/$Ni(OH)_2$-0.9	/	100.7 at 0.287 kW kg^{-1}	[4]
Ni-NiO heterostructured nanosheets	0.0066 at 2.0 mW cm^{-2}	/	[5]
Ni-mMeSA//Zn@CC	0.30 at 33.72 mW cm^{-2}	125 at 14.03 kW kg^{-1}	[6]
NiO nanoflakes	/	94.5 at 1.2 kW kg^{-1}	[7]
Co-doped $Ni(OH)_2$@NNA	0.3565 at 4.128 mW cm^{-2}	148.54 at 1.72kW kg^{-1}	[8]
ZnO nano-wires	0.000027 at 0.014 mW cm^{-2}	/	[9]
Ni-OA-3 hierarchical superstructure	0.42 at 0.86 mW cm^{-2}	138.75 at 0.29 kW kg^{-1}	[10]
NC-NiCo-PBA	0.33 at 1.74 mW cm^{-2}	132 at 0.69 kW kg^{-1}	[11]
H-NiCo-MOF@AHC	**0.37 at 1.52 mW cm^{-2}**	**148 at 0.61 kW kg^{-1}**	**This work**

a) E_A: areal energy density; b) E_G: gravimetric energy density.

References

[1] T. Chen, Y. Bai, X. Xiao and H. Pang, *Chem. Eng. J*., 2021, **413**, 127523.

[2] Y. Zeng, Z. Lin, Y. Meng, Y. Wang, M. Yu, X. Lu and Y. Tong, *Adv. Mater*., 2016, **28**, 9188.

[3] G. Zhang, H. Yang, H. Zhou, T. Huang, Y. Yang, G. Zhu, Y. Zhang and H. Pang, *Angew. Chem. Int. Edit*., 2024, **63**, e202401903.

[4] J. Liu, M. Chen, L. Zhang, J. Jiang, J. Yan, Y. Huang, J. Lin, H. J. Fan and Z. X. Shen, *Nano Lett.*, 2014, **14**, 7180.

[5] Y. Zeng, Y. Meng, Z. Lai, X. Zhang, M. Yu, P. Fang, M. Wu, Y. Tong and X. Lu, *Adv. Mater.*, 2017, **29**, 1702698.

[6] Y. Su, J. Hu, G. Yuan, G. Zhang, W. Wei, Y. Sun, X. Zhang, Z. Liu, N.-T. Suen, H.-C. Chen and H. Pang, *Adv. Mater.*, 2023, **35**, 2307003.

[7] C. Guan, W. Zhao, Y. Hu, Q. Ke, X. Li, H. Zhang and J. Wang, *Adv. Energy Mater*., 2016, **6**, 1601034.

[8] C. Xu, J. Liao, C. Yang, R. Wang, D. Wu, P. Zou, Z. Lin, B. Li, F. Kang and C.-P. Wong, *Nano Energy*, 2016, **30**, 900.

[9] J. Bae, M.K. Song, Y.J. Park, J.M. Kim, M. Liu and Z. L. Wang, *Angew. Chem. Int. Ed.*, 2011, **50**, 1683.

[10] F. Sun, T. Chen, Q. Li, H. Pang, *J. Colloid Interf. Sci.*, 2022, **627,** 483.

[11] Z. Qiu, S. Zhang, H. Lin, X. Lu, Z. Meng, S. Wang, S. Cao, Q. Li, T. Wang, Y. Xu, M. Shakouri, Y. Pi and H. Pang, *Green Chem. Eng.*, 2025 https://doi.org/10.1016/j.gce.2025.08.002.